ingegneria sismica
International Journal of Earthquake Engineering
Anno XLIII - Num. 1 - 2026

GIS-based Multi-source Reanalysis Data Fusion in Complex Terrain Scenic Resource Assessment

Mi Zhang[1], *Qiang Xiao*[1], *Jingbo Ma*[1], *Jian Zhang*[2,*] *and Yuguo Chen*[2]

[1] New-Type Power System Construction Center, State Grid Chongqing Economic and Technology Research Institute, Chongqing, 401121, China
[2] Beijing Tsintergy Technology Co., Ltd., Beijing, 100080, China

SUMMARY: *In this study, a deep learning-based fusion assessment method for wind and solar resource data is proposed to address the problem of poor accuracy of wind and solar resource assessment under complex terrain. The method adopts Kalman filter for the fusion of wind and solar resource reanalysis data, and introduces convolutional network to extract the deep features of multi-source data. Then parallel spatio-temporal axial attention is introduced to learn the long-time dependency and spatial correlation relations. The high precision reconstruction and spatial distribution prediction of scenery variables are realized by the decoder structure, meanwhile, based on the multi-task learning framework, it makes the model optimize the assessment tasks of wind speed and light simultaneously, which improves the assessment efficiency of the model. The experimental results show that the model is able to effectively improve the assessment accuracy of wind and scenery resources in complex terrain, and the average errors of both the angle of attack and the side-slip angle are reduced by more than 60%. In the comparison of SVR and other classical models, this paper's algorithm has the best overall performance in all assessment tasks, especially in the fusion data set of scenery variables, the error is reduced by 2.72%~7.05% compared with the comparison model. It proves the effectiveness and superiority of this paper's model in the assessment of complex terrain scenery resources, which can provide reliable technical support for scenery resources planning.*

KEYWORDS: *Multi-source reanalysis data fusion; Transformer; Axial attention; Scenic resource assessment; Kalman filtering*

1 Introduction

In recent years, in order to further expand the mining and use of renewable energy, the development of complex terrain has become a major development direction [1]. However, there are many risks and challenges in the development process. In order to safely and efficiently develop renewable energy sources such as wind power and photovoltaic projects, and at the same time to ensure the balance between economic benefits and ecological environmental protection, the assessment of landscape resources in complex terrains has become a necessary and important part [2-4]. Unlike flat terrain, complex terrain has a variety of geomorphological features such as mountains, valleys, hills, etc., which makes the traditional assessment methods need to record the wind resource data at different heights and at different times, which is inefficient and has low accuracy and stability [5-7]. In order to improve the efficiency and accuracy of the assessment, the multi-source data fusion aspect of geographic information

---

*zhangjujs126@.com

https://doi.org/10.65102/is2026241

systems (GIS) has been gradually applied [8].

GIS is an emerging technology based on computers, which is a platform used to specialize in the processing of information associated with geographic location and spatial distribution and its attribute data, mainly to solve the problems related to location and spatial distribution, which can effectively store massive information and represent the results of the processing in the form of maps, graphs and data [9-12]. With the arrival of the information age, multi-source reanalysis data fusion an important topic in the field of GIS. Multi-source reanalysis data fusion of GIS is the process of integrating reanalysis data from different channels such as satellite remote sensing, aerial photography, ground measurements, social media, etc., such as temperature, precipitation, etc., to generate a set of more comprehensive and accurate climate datasets, so as to provide better decision support for the scenery resources of the complex terrain assessment to provide better decision support [13-16].

In this paper, a deep learning framework that integrates the Transformer encoder and the spatio-temporal axial attention mechanism is introduced to construct a multi-source data fusion assessment model for wind and light resources. The method captures the spatial dependence of wind and light variables through the spatio-temporal axial attention mechanism, and utilizes the Transformer encoder to achieve efficient fusion of multi-source observational data and deep feature extraction, in order to enhance the model's ability to model the distribution of the wind field and solar radiation under complex terrain. In order to verify the reliability of the model in this paper, experiments were conducted on the constructed historical wind variable dataset, historical light variable dataset and historical scenery variable sequence fusion dataset, and a multi-dimensional comparison was made between the model in this paper and the mainstream models such as LSTM, so as to make a comprehensive assessment of the performance of the model in terms of the estimation accuracy and the stability of the error.

2 GIS-based fusion of multi-source reanalysis data for scenic resource assessment

2.1 Complex Terrain Scenic Resource Data and MCP Analysis Methods

2.1.1 Complex terrain scenic resource data

NCEP/NCAR data is a reanalysis dataset jointly launched by the National Centers for Environmental Prediction (NCEP) and the National Center for Atmospheric Research (NCAR), which provides long-term complex terrain wind and scenic resource data every 2.5-2.5 latitude and longitude, 6h by 6h globally, including: wind data, temperature, heat fluxes, etc., and it is the longest reanalysis data with the longest time series available, which is widely used in various researches on climate diagnostic analysis, moisture cycle and so on. It is the longest time series of reanalysis data available, and is widely used in climate diagnosis and analysis, moisture cycle and other aspects of research, and in climate simulation and prediction research as the initial field and boundary conditions of the regional climate model, used to test the simulation results.The wind data in the NCEP/NCAR data include: wind data in different pressure layers from 10 to 1000hPa, near-surface layer wind data, and 10m elevation wind data, among which the 10m elevation data are the reference data. forecast data, which are 6h behind the reference time in time and distributed according to Gaussian grid.

The solar radiation data integrating satellite remote sensing inversion and terrain correction include: total radiation intensity (GHI) and direct scattering separated radiation (DNI/DHI), slope radiation distribution after slope orientation correction, sunshine hours and radiation attenuation coefficient influenced by terrain shading effect, and radiation data with high temporal and spatial resolution. The high temporal and spatial resolution radiation data are applicable to the assessment of light resources in complex terrain such as mountains, hills and plateaus.

2.1.2 MCP analysis methodology

NCEP/NCAR wind data can reflect the field wind conditions to a certain extent, however, the correlation will be different according to the changes of the field wind conditions, and considering that the data is a 6h average data, the commonly used MCP analysis methods, such as linear regression method and matrix method, are not suitable for the MCP analysis of NCEP/NCAR data because of the high requirement of the time resolution of long-term data. In this study, based on the characteristics of NCEP/NCAR data and with reference to the analysis results of foreign research institutes, a MCP analysis method of NCEP/NCAR data based on normalization theory is proposed - wind index method. The wind index is the value corresponding to the normalization of the average value of the output power of WTGs in a certain period of time. The wind index method is an MCP analysis method for the average value of the output power of WTGs, which does not consider the correlation of the wind direction, does not correct the short-term data, and directly applies the short-term data to calculate the annual electricity generation of the planned wind farms, and then corrects the annual electricity generation according to the proportionality of the wind indices of the long and short-term data. Correction. Compared with other MCP analysis methods, the wind index method is a relatively simple and most stable calculation method, especially for the long-term data accuracy is poor, other analysis methods can not be used, this method can often obtain satisfactory results.

The wind index method divides the long-term data and short-term data into long-term data W_{rf}, data W_{rc} in the long-term data in the same time period as the short-term data used for calculation, short-term data W_{sf}, and short-term data used for calculation W_{sc}, and firstly, calculates the average output power corresponding to the above four types of data according to equation (1):

$$E_j = \sum_{i=1}^{N} P(u_i) / N \tag{1}$$

where E_j is the average output power of a wind measurement period; $P(u_i)$ is the power curve of alternative WTGs or standard WTGs; N is the number of wind measurements in the wind measurement period; u_i is the i th wind measurement data.

Let the wind index I_{rf} of $I_{rf} = 100$, the wind index of W_{rc} can be obtained according to the following equation:

$$I_{rc} = \frac{E_{rc} \cdot 100}{E_{rf}} \tag{2}$$

One very important assumption to make at this point is to assume that W_{rc} has the same wind index as W_{sc}, as shown in the following equation:

$$I_{sc} = I_{rc} \tag{3}$$

After obtaining I_{sc} from Eq. (3), the wind index I_{sf} of W_{sf} can be found according to the following equation:

$$I_{sf} = \frac{E_{sf} \cdot I_{sc}}{E_{sc}} \tag{4}$$

Substituting I_{sf} gives the correction coefficients used to correct the annual generation of the wind farm:

$$C_{sf} = \frac{100}{I_{sf}} \tag{5}$$

The correction factor C_{sf} for the annual generation of the planned wind farm is the final calculation result of the wind index method. When applying the wind index method for MCP analysis, whether or not the wind index is the same (or similar) is an important factor affecting the results of the MCP analysis. The validity of the wind index calculation results can usually be measured based on the correlation comparison between W_{rc} and W_{sc} monthly average wind indices.

2.2 Kalman filter-based data fusion for reanalysis of scenic resources

Kalman filtering is an optimized regression data processing algorithm, which has been widely used in all major fields, such as system control of intelligent robots, military radar systems and missile capture. In recent years, Kalman filtering is even applied to other popular fields, such as image recognition, fingerprint recognition, etc., has also been fully developed.

The basic principle of Kalman filtering is to assume that the best estimate of the point is under the condition of having the value of the point according to the previous point, the estimation method it utilizes is the statistical algorithm, as a traditional mathematical fitting, Kalman filtering has the advantage of requiring little memory and running fast.

The Kalman filter model is as follows:

$$\hat{x}_{\bar{k}} = A \cdot \hat{x}_{k-1} + B \cdot u_{k-1} + w_k \tag{6}$$

where $\hat{x}_{k-1}$ and $\hat{x}_k$ denote the a posteriori state estimates, i.e., the updated results, also called the optimal estimates, at $k-1$ and k points, respectively; and $\hat{x}_{\bar{k}}$ denotes the a priori state estimates at k points, i.e., the predicted results at k points based on the optimal estimates at the previous point; w_k is the process noise and is assumed to conform to a mean of zero; A is the state transfer matrix; B is the matrix that transforms the inputs into states; and u_{k-1} is the control quantity at the previous point, or zero if it is not available.

$$P_{\bar{k}} = A \cdot P_{k-1} \cdot A^T + Q \tag{7}$$

where P_{k-1} and P_k denote the a posteriori estimated covariance at $k-1$ and k points, respectively; $P_{\bar{k}}$ is the a priori estimated covariance at the k points (the covariance of $\hat{x}_{\bar{k}}$); and Q is the process excitation noise covariance (the covariance of the system process).

$$K_k = \frac{P^{\bar{k}} \cdot H^T}{H \cdot P_{\bar{k}} \cdot H^T + R} \tag{8}$$

where H is the state variable to measurement (observation) transition matrix; R is the measurement noise covariance; and K_k is the filter gain matrix.

$$\hat{x}_k = \hat{x}_{\bar{k}} + K_k \left(z_k - H \cdot \hat{x}_{\bar{k}} \right) \tag{9}$$

where $\left(z_k - H\hat{x}_{\bar{k}} \right)$ is the residuals of the actual and predicted observations; and z_k is the measurements (observations), which are the inputs to the filter.

$$P_k = \left(I - K_k \cdot H \right) \hat{x}_{\bar{k}} \tag{10}$$

Kalman filter fusion is limited by the structure of the model, and cannot add different types of data for the training of the model like deep learning models. In this study, only the scenery resource data of complex terrain is input, and its fusion process is shown in Figure 1.

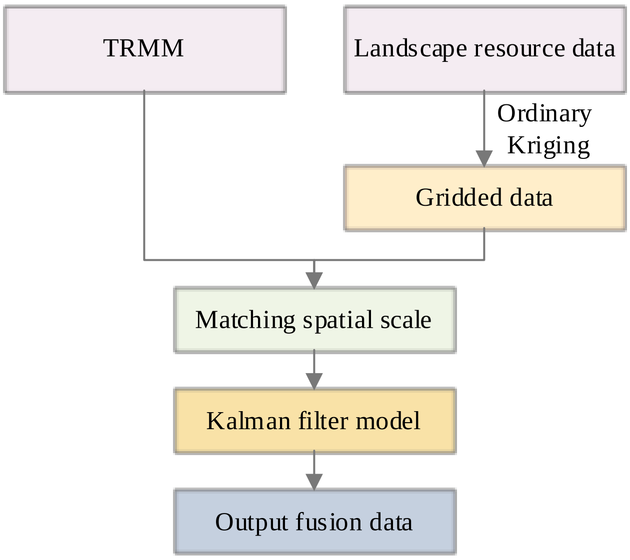

Figure 1: Kalman filter fusion flow chart

2.3 Network Model for Assessing Landscape Resources in Complex Terrain

2.3.1 Problem definition and model overview

Based on the spatial resolution of the reanalyzed data and the time intervals at which they were sampled, the Complex Terrain Scenic Resource Assessment data is a set of sequential data with a specific spatial and temporal resolution.

Based on the above representation, the complex terrain and scenic resource assessment task can be formulated as a sequence prediction problem. Specifically, given a historical complex terrain scenic resource assessment sequence $X = \left\{ M^{t-T_{in}+1}, M^{t-T_{in}+2}, \cdots, M^{t} \right\}$ predicts the complex terrain scenic resource data for the future period $\hat{Y} = \left\{ \hat{M}^{t+1}, \hat{M}^{t+2}, \cdots, \hat{M}^{t+T_{out}} \right\}$ where

T_{in}, T_{out} respectively denote the sequence length of the input and the sequence length of the output. The goal of this paper is to construct a deep learning model that makes the predicted sequence $\hat{Y}$ close to the real complex terrain scenic resource assessment data $Y = \left\{M^{t+1}, M^{t+2}, \cdots, M^{t+T_{out}}\right\}$.

Overall, the model proposed in this paper consists of three parts: multimodal feature fusion network, Transformer-based encoder-decoder network and spatial regression network. Notation F^t denotes the feature map output from the complex terrain scenery resource data through the multimodal fusion network at moment t. On the basis of multimodal feature fusion, the Transformer encoder-decoder structure further models the spatial and temporal dependencies among the complex terrain scenic resource data. The decoder outputs the final feature representation $\left\{Z^{t+1}, Z^{t+2}, \cdots, Z^{t+T_{out}}\right\}$ Finally, spatial regression network converts the spatio-temporal feature maps of the decoder output into the final predictions $\left\{\hat{M}^{t+1}, \hat{M}^{t+2}, \cdots, \hat{M}^{t+T_{out}}\right\}$.

2.3.2 Multimodal feature fusion networks

In order to learn the coupling relationship between different modalities, and at the same time to effectively fuse the multimodal features, this paper designs a multimodal feature fusion network, which has the following main features:

(1) Structurally, a multi-branch hierarchical fusion strategy is adopted. The network consists of four modal branches and one fusion branch.

(2) Technically, a feature fusion method based on a gating mechanism is used. The input of each layer in the fusion branch contains the current features R_j^t, T_j^t, U_j^t, V_j^t of each modal branch, and the current fusion feature F_j^t, and the initial fusion feature is set to zero.

$$G_j^F, G_j^R, G_j^T, G_j^U, G_j^V = \sigma\left(M_{\theta_j}\left(F_j^t, R_j^t, T_j^t, U_j^t, V_j^t\right)\right) \tag{11}$$

$$\begin{aligned} F_{j+1}^t = {} & G_j^F \otimes F_j^t + G_j^R \otimes R_j^t + G_j^T \otimes T_j^t \\ & + G_j^U \otimes U_j^t + G_j^V \otimes V_j^t \end{aligned} \tag{12}$$

where G_j^R, G_j^T, G_j^U, G_j^V denote the corresponding gating weights of each modality, and G_j^F denotes the gating weight of the current multimodal fusion feature. In addition, σ denotes the Sigmoid function, which is a commonly used gating activation function.

2.3.3 Transformer-based encoder-decoder network

Based on the spatial features extracted from the multimodal fusion network, the spatio-temporal dependencies between the data are further learned through the Transformer encoder-decoder. The attention mechanism is the core of the Transformer model, which can be described as the process of mapping a query and a set of “key-value pairs” to an output. Given a set of query matrices $Q \in \mathbb{R}^{N_q \times d}$, and key-value matrices $K, V \in \mathbb{R}^{N_k \times d}$, the output of the attentional operation is as follows:

$$Attention\left(Q, K, V\right) = soft\max\left(\frac{QK^T}{\sqrt{d}}\right)V \tag{13}$$

When $Q = K = V$, it is called a self-attention mechanism. Multi-attention is an extension of the attention mechanism that runs k attention operations in parallel by projecting queries, keys, and values to different subspaces via a learnable k set of linear transformations. The outputs of these k attentions are then spliced together to obtain the final output via a learnable linear transformation:

$$MultiHeadAttention\left(Q,K,V\right) = Concat\left(h_1,h_2,\cdots,h_k\right)W^O \tag{14}$$

$$h_i = Attention\left(QW_i^Q, KW_i^K, VW_i^V\right) \tag{15}$$

where $W_i^Q, W_i^K, W_i^V \in \mathbb{R}^{d\times d_h}$ are the parameter matrices for the linear transformations of query, key, and value, respectively, and $W^O \in \mathbb{R}^{kd_h\times d}$ is the parameter matrix of the final linear transformation for the multi-head attention mechanism. In general, d_h is often set to d/k.

The encoder-decoder framework based on the attention mechanism is widely used in sequence-to-sequence prediction tasks to learn the correlations between elements in a sequence.

The attention mechanism can effectively model long-range dependencies, but it is computationally very expensive for spatio-temporal sequences. The difference is that attention is implemented separately along three directions: vertical (latitudinal), horizontal (longitudinal), and temporal axes of space. The axial attention designed in this paper is a spatio-temporal axial attention mechanism in a parallel manner to enhance the training and inference speed of the model, and the structure of this attention mechanism is shown in Fig. 2. Computationally, the attention operation is executed independently along the three dimensions, so the computational complexity required for each position on the spatio-temporal feature map is reduced from $O\left(T\times H\times W\right)$ to $O\left(T+H+W\right)$. At the same time, the feature after the attention operation still maintains the global sensory field, and the axial attention output $\tilde{z}_{i,j,t}$ for a specific position $\left(i,j,t\right)$ is computed as follows:

$$\tilde{z}_{i,j,t}^1 = soft\max\left(\frac{q_{i,j,t}K_1^T}{\sqrt{d}}\right)V_1 \tag{16}$$

$$\tilde{z}_{i,j,t}^2 = soft\max\left(\frac{q_{i,j,t}K_2^T}{\sqrt{d}}\right)V_2 \tag{17}$$

$$\tilde{z}_{i,j,t}^3 = soft\max\left(\frac{q_{i,j,t}K_3^T}{\sqrt{d}}\right)V_3 \tag{18}$$

$$\tilde{z}_{i,j,t} = \tilde{z}_{i,j,t}^1 + \tilde{z}_{i,j,t}^2 + \tilde{z}_{i,j,t}^3 \tag{19}$$

where $q_{i,j,t}$ is the corresponding query vector, $K_1,V_1 \in \mathbb{R}^{H\times d}$ is the corresponding key-value matrix along the vertical latitudinal direction, $K_2,V_2 \in \mathbb{R}^{W\times d}$ is the corresponding key-value matrix along the horizontal longitudinal direction, $K_3,V_3 \in \mathbb{R}^{T\times d}$ are the corresponding key-value matrices along the time direction.

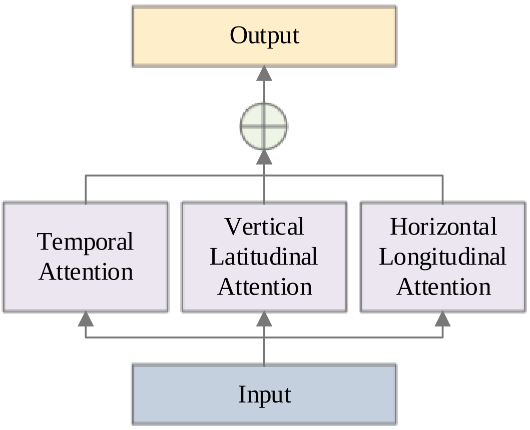

Figure 2: Spatio-temporal axial attention

The encoder-decoder construction is shown in Fig. 3. The encoder is made up of multiple identical layers stacked on top of each other. Each layer consists of two sub-layers, i.e., the spatio-temporal axial attention layer and the convolutional feedforward network.

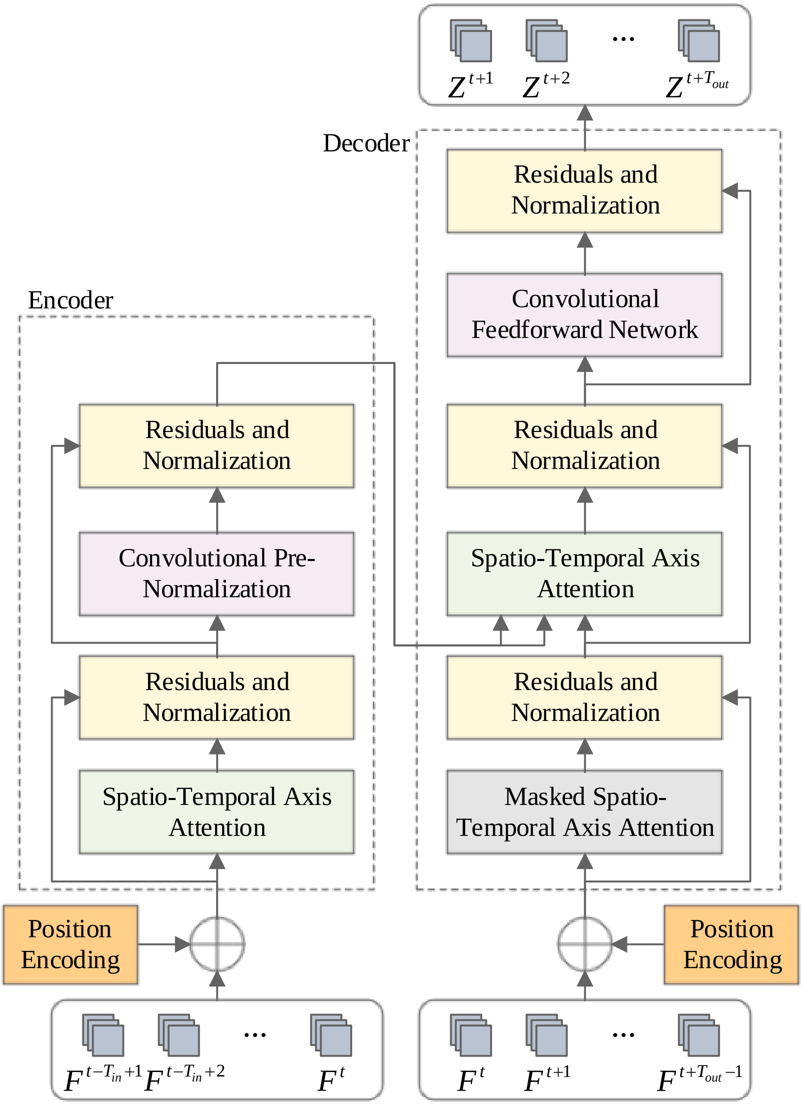

Figure 3: Encoder-decoder based on Transformer

The decoder also consists of multiple identical layers stacked on top of each other, each consisting of three sublayers. Structurally, in addition to the two sublayers implemented in the encoder, the decoder inserts an encoder-decoder cross-attention layer between these two sublayers.

Similar to the working mechanism of the original Transformer, in the testing phase the model works in an autoregressive manner, i.e., each prediction in the target sequence is generated by iteration.

2.3.4 Location coding

Recurrent neural networks process the input sequences one by one, thus ensuring temporal backward and forward order, but the attention mechanism abandons sequential operation due to parallel computing. In the task of complex terrain scenery resource assessment, a three-dimensional tensor is needed to represent the positional relationship since this paper applies the attention mechanism to the time axis, vertical and horizontal directions in space. Similar to the two-dimensional position encoding in images, this paper uses a learning strategy to learn three groups of position encoding. Here, the dimension of each group of position encoding is set to $d/3$, and d is the dimension of the feature in the attention module. Based on the position coordinates of the input tensor, the three sets of position encoding will be connected together to represent the final position embedding representation.

2.3.5 Spatial regression networks

The spatial regression network consists of an anti-convolution layer with an activation function. The inverse convolution operation is the opposite of the traditional convolution, which can realize the up-sampling of the input data. The spatial regression network, on the other hand, maps the feature maps generated by the decoder $\left\{Z^{t+1}, Z^{t+2}, \cdots, Z^{t+T_{out}}\right\}$ to the meteorological state space with greater spatial resolution. After obtaining the prediction results, training is performed by minimizing the mean square error between the predicted and true values, and the corresponding loss function is defined as:

$$L\left(Y,\hat{Y}\right)=\frac{\left\|Y-\hat{Y}\right\|^{2}}{E\times P\times H\times W} \tag{20}$$

where Y is the real complex terrain scenery resource assessment sequence, $\hat{Y}$ is the predicted complex terrain scenery resource assessment sequence, E is the number of meteorological modes, P is the number of isobaric layers, and H and W denote the number of grids in the longitudinal and latitudinal directions, which are related to the size of the area to be predicted and the spatial resolution.

3 Results of data fusion and assessment of scenic resources in complex terrain

3.1 Wind speed fusion simulation experiment in complex terrain scenery resources

In order to verify the effectiveness of the above algorithm, numerical simulation is used to validate the algorithm. The wind speed in the complex terrain scenery resource considers the mean wind and atmospheric turbulence, and the component of the mean wind on the x/y/z axes varies from -30 to 30 m/s. Both pressure sensor noise and INS system noise are modeled as first-order Markov processes. The barometric observation noise is 16 Pa at the same horizontal plane, and the wind speed observation data use the data observed 3.2 hours before the flight, and the observation noise is Gaussian white noise. Because the observation data of scenery resources in complex terrain are divided into wind speed data and light resource data, the filtering effect based on Kalman filter after fusion of wind speed data is analyzed in the simulation experiment.

Under the above simulation conditions, the estimated values and errors of the metrics of the fused wind speed observations and those of the fused wind speed observations and those of the fused wind speed observations without fusing any complex terrain scenic resource observations are shown in Fig. 4, and Figs. (a) to (f) show the estimated curves of the angle of attack and the side-slip angle, the error curves corresponding to the angle of attack and the side-slip angle, the estimated curves of the Mach number and their error curves, respectively.

Considering the wind speed case, the fusion estimation algorithm proposed in this paper is able to obtain the estimated values of angle of attack, sideslip angle and Mach number throughout the estimation process after fusing the wind speeds from the wind and light resource observation data of the complex terrain.

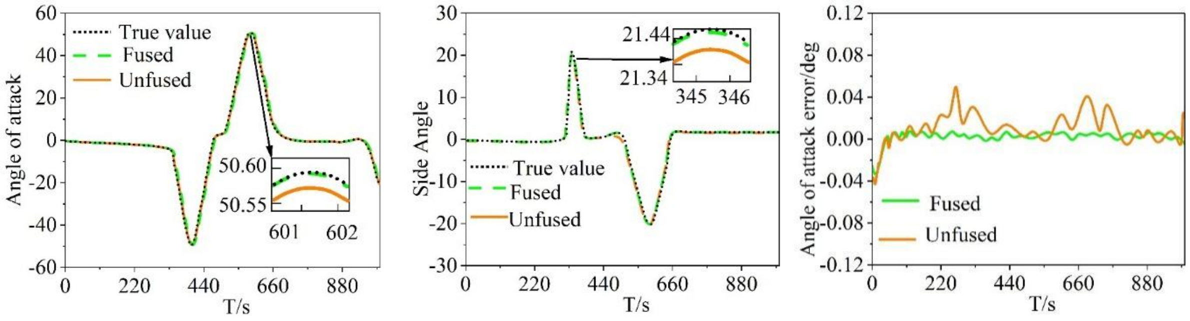

(a)Angle estimation curve (b)Side Angle estimate (c)Angle estimation error

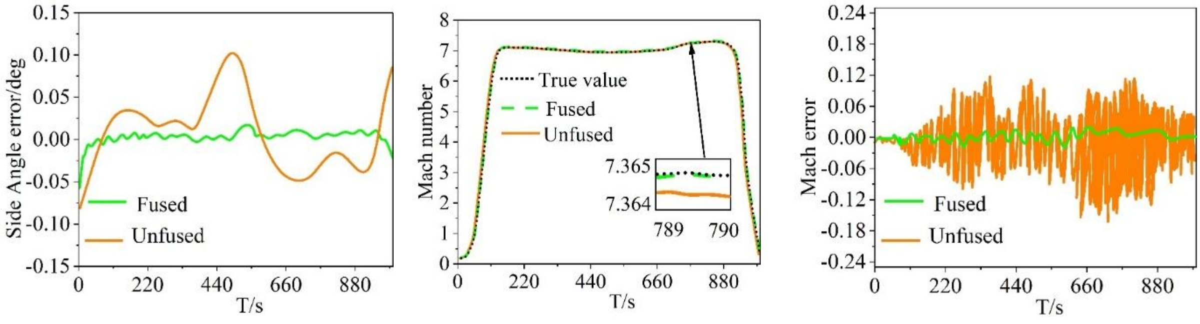

(d)Side Angle error (e)Mach number estimate (f)Mach number error

Figure 4: The value and error of the index of fusion wind speed information

Moreover, relative to the estimation algorithm of complex terrain scenery resource data fused with FADS/INS only, the algorithm proposed in this paper after fusing the wind speed of complex terrain scenery resource observation data has significantly improved the accuracy in the estimation of the angle of attack, sideslip angle, and Mach number. In order to further quantitatively analyze the error situation, the maximum value (the maximum value of the absolute value of the error) and the average value (the average value of the absolute value of the error) of the estimation errors of the angle of attack, side slip angle and Mach number are calculated, and the error statistics of the angle of attack, side slip angle and Mach number are shown in Table 1.

From the data in the table, the following conclusion can be obtained: compared with the fusion of FADS and INS data only, after the fusion of complex terrain and scenery resource observation data, the average error of angle of attack and the average error of side slip angle are reduced by 66.42% and 83.59%, respectively, and the fusion of complex terrain and scenery resource observation data has an obvious effect on the improvement of the estimation accuracy. And the integration of wind speed observation also improves the estimation accuracy of Mach number very obviously. The above are the statistical properties of angle of attack, sideslip angle, Mach number and barometric altitude.

Table 1: Error statistics

Error		Maximum value	Mean
Angle of attack error	Unintegrated observed data	0.0795	0.0265
	The EKF that combines wind velocity observation	0.0578	0.0089
	Estimation range	-55~55°	
Side Angle error	Unintegrated observed data	000859	0.0256
	The EKF that combines wind velocity observation	0.0421	0.0042
	Estimation range	-25~25°	
Mach number error	Unintegrated observed data	0.0236	0.0045
	The EKF that combines wind velocity observation	0.0088	0.0012
	Estimation range	0.1~7.5	

3.2 Results of data fusion assessment for complex terrain scenic resources

3.2.1 Performance of the models in different terrain types

In this chapter, the corresponding simulation analysis is carried out for the data of each model and algorithm under different complex terrain types in the test set, in order to observe the performance of each model and algorithm under different complex terrain types, and the terrains involved in the table are mountains, hills, valleys, ridges, plateaus, basins, canyons, slopes, terraces, coastal complex terrains, karstic terrains, and volcano terrains, and the above complex terrains are numbered, and the numbering is A1 ~A12. Table 2 shows the MSE values of each model under different complex terrain types, where WT-LSTM, Adv-Trans and Ours denote the Wavelet-LSTM algorithm, Adv-Transformer model and the predictive deep learning model based on multimodal fusion in this paper, respectively.

The error values of each model are the largest in three complex terrain conditions: hill, plateau and volcano. This paper's algorithm performs best in the hilly, ridge and canyon complex terrain, with MSEs less than 1, and maintains better results in other cases, proving the effectiveness of the model.

Table 2: MSE values of various models in different complex terrain types

Complex terrain type	Prediction model					
	SVR	BPNN	LSTM	WT-LSTM	Adv-Trans	Ours
A1	1.1947	1.0598	1.0370	1.0227	1.2023	0.8904
A2	5.7838	5.2906	5.6319	5.5873	5.3277	5.1389
A3	3.9414	4.0192	4.1699	4.0642	3.7662	3.6940
A4	1.5551	1.2750	1.3071	1.2936	1.2733	0.9351
A5	6.3127	5.4009	5.6107	5.5272	5.4515	5.2116
A6	3.4411	3.4914	3.5465	3.4628	3.2413	3.1597
A7	0.9935	1.0547	1.0522	1.0544	1.0870	0.7694
A8	3.7812	3.5603	3.7532	3.8220	3.6817	3.4572
A9	2.5729	2.7931	2.7237	2.8194	2.6548	2.4614
A10	1.7318	1.9422	1.6995	1.6490	1.8758	1.5407
A11	3.7627	3.7926	3.6953	3.6195	3.5318	3.5152
A12	5.2056	5.6750	5.4472	5.5150	5.2570	5.1561

3.2.2 Multi-source heterogeneous feature fusion analysis

In order to verify the effect of fusing multi-source heterogeneous features as inputs on the prediction accuracy of the model, this chapter constructs three datasets, dataset W (historical wind variable sequences), dataset L (historical light variable sequences), and dataset F (fusion dataset of historical wind variable sequences and light variable sequences), and utilizes the three datasets to adequately train the models and algorithms and test the accuracy of the models and algorithms on the test set, respectively. Testing. Table 3 shows the MSE, MAE and MSLE values of each model on the three datasets.

The error values of each neural network model except the SVR model on the fusion dataset of the historical wind variable series and the historical light variable series are smaller than those on the single dataset, indicating that each neural network model extracts the correlation features between the two single datasets from the fusion dataset, which makes the model's prediction more accurate.

The models with the smallest MSE values on the historical wind-variable series dataset, the historical light-variable series dataset, and the fusion dataset are the SVR model, the Ours algorithm, and the Ours algorithm, respectively, and the smallest MSE values on the three datasets are 2.7005, 2.8622, and 2.5239. Meanwhile, each neural network model except SVR model performs best on the fusion dataset, second best on the historical light variable sequence dataset and worst on the historical wind variable sequence dataset. While in the SVR model, the best performance was on the historical wind variable sequence dataset, followed by the fusion dataset and the worst performance on the historical light variable sequence dataset. For each neural network model, it extracts features from the historical optical variable sequence that are more relevant to the moment to be predicted, and thus each model outperforms the historical wind variable sequence dataset on the historical optical variable sequence dataset. The algorithm in this paper outperforms the simple LSTM model and the Transformer model on the fused dataset, demonstrating the effectiveness of the deep learning model for prediction based on multimodal fusion.

Table 3: The models are shown in different data sets

Model	Error indicator	The three Numbers are set by the set		
		W	L	F
SVR	MSE	2.7005	3.2947	2.7018
	MAE	0.7141	0.7284	0.7142
	MSLE	0.0388	0.0493	0.0387
BPNN	MSE	3.5928	2.9222	2.6290
	MAE	1.0002	0.7439	0.8068
	MSLE	0.0628	0.0489	0.0683
LSTM	MSE	3.6456	2.8677	2.6317
	MAE	0.9738	0.7058	0.7193
	MSLE	0.0587	0.0502	0.0422
Wavelet-LSTM	MSE	3.7087	2.8949	2.6117
	MAE	0.9909	0.7028	0.7247
	MSLE	0.0656	0.0498	0.0425
Adv-Transformer	MSE	3.9254	2.9762	2.5926
	MAE	1.0111	0.7084	0.7604
	MSLE	0.0641	0.0530	0.0382
Ours	MSE	3.8026	2.8622	2.5239
	MAE	0.9688	0.6892	0.7049
	MSLE	0.0553	0.0499	0.0392

3.2.3 Model convergence analysis

In this chapter, the errors of each model and algorithm on the training and test sets are recorded during the training process, so as to determine whether the models have converged or not, and the model with the smallest error on the test set is saved for subsequent research. Figure 5~Figure 7 represent the loss function curves of each neural network model on the historical wind variable sequence dataset, the historical light variable dataset and the fusion dataset, respectively, where WT-LSTM, Adv-Trans and Ours represent the Wavelet-LSTM algorithm, the Adv-Transformer model and the algorithm of this paper, respectively.

On the historical wind variable series dataset, the error values of the LSTM model, Wavelet-LSTM algorithm, Adv-Transformer model and this paper's algorithm start to increase soon after the number of iterations to reach the optimal result and the model starts to overfit, while the error curve of the BPNN model is smoother after reaching the minimum value. On the historical PV power dataset, the error curves of the LSTM model, the Wavelet-LSTM algorithm and the Adv-Transformer model start to increase after the number of iterations to reach the optimal result, and all three algorithms start to increase the error curves around the 40th iteration while the error curves of the BPNN model and the algorithms of the present paper remain smooth after reaching the minimum value; on the fusion dataset, the error values of BPNN model, LSTM model, Wavelet-LSTM algorithm and Adv-Transformer model start to increase soon after the number of iterations to reach the best result, and the model is overfitted, while the error function curves of this paper's algorithm have a small change in general after reaching the minimum value.

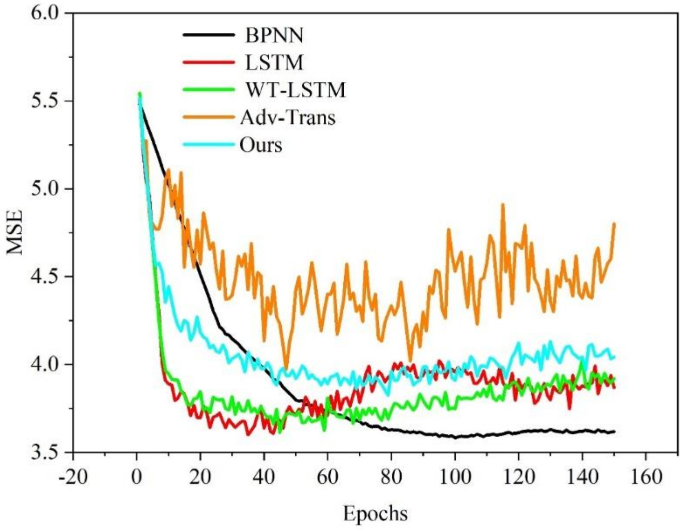

Figure 5: Historical wind variable sequence data set

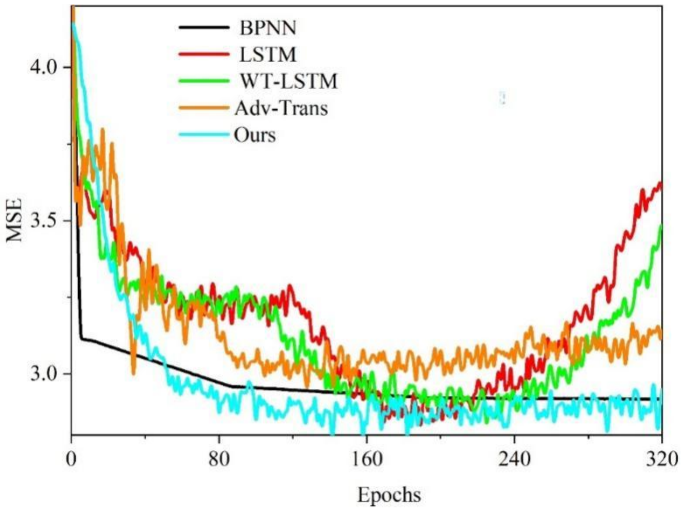

Figure 6: Historical light variable sequence data set

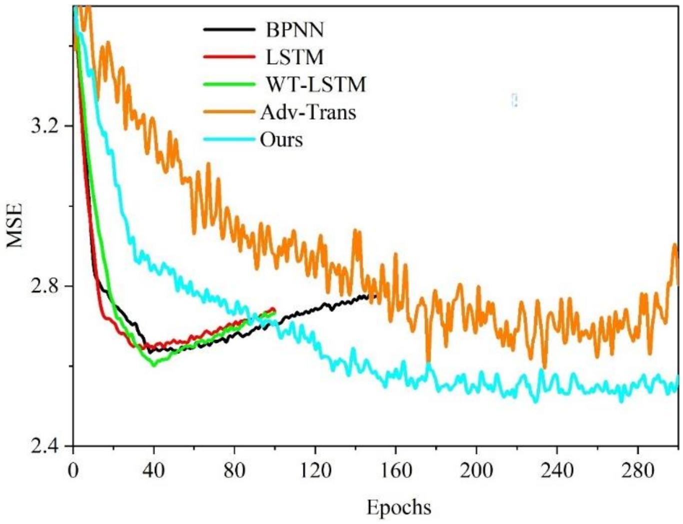

Figure 7: Historical fusion variable sequence data set

4 Conclusion

Aiming at the difficulties of scenery resource assessment under complex terrain, this paper proposes a complex terrain scenery resource assessment model based on multi-source reanalysis data fusion, and the constructed model is divided into two parts: modal correlation capture and data spatio-temporal dependence modeling.

The systematic error of scenery resource assessment is significantly reduced by using the multi-source data fusion technique, and the average error of angle of attack and the average error of side-slip angle are reduced by 66.42% and 83.59%, respectively, which proves that the fusion of complex terrain scenery resource observation data plays a key role in improving the accuracy of complex terrain scenery resource assessment.

On the same dataset, SVR model, BPNN model, LSTM model, Wavelet-LSTM algorithm, Adv-Transformer model, etc. and this paper's model are trained and tested in comparison, and the MSE values of each model under different complex terrain conditions are analyzed, and the results show that this paper's algorithm has the best performance in terms of comprehensive performance.

On the constructed historical wind variable dataset, historical light variable dataset, and historical wind variable and light variable fusion dataset, the relevant performance of each model is discussed and the data fusion effect and convergence results of each model are verified. The simulation results show that this paper's algorithm performs best on the most challenging wind-variable fusion dataset, and the MSE of this paper's algorithm on the wind-variable fusion dataset is reduced by 7.05%, 4.16%, 4.27%, 3.48%, and 2.72%, respectively, when compared with comparative models, such as the SVR model and the BPNN model. And the error function curve of this paper's model is generally more stable after reaching the minimum value, without overfitting phenomenon, which confirms the excellent performance of this paper's algorithm in dealing with multi-source in analyzing the fusion dataset.

Funding

This research was supported by the State Grid Chongqing Electric Power Company Economic Research Institute 2025 Research Plan: New Energy Resource Survey and Development Impact Research Service in Chongqing (SGCQJY00XXJS2500035).

References

[1] Zhao, W., & Li, A. (2015). A review on land surface processes modelling over complex terrain. Advances in Meteorology, 2015(1), 607181.

[2] Wang, Q., Luo, K., Wu, C., Zhu, Z., & Fan, J. (2022). Mesoscale simulations of a real onshore wind power base in complex terrain: Wind farm wake behavior and power production. Energy, 241, 122873.

[3] Mo, L., Chen, J., & Xie, Y. (2021). Assessment of landscape resource using the scenic beauty estimation method at compound ecological system. Environmental Science and Pollution Research, 28(5), 5892-5899.

[4] Jia, Z., & Qin, A. (2022). Evaluation of the spatial distribution of scenic resources based on 3S technology: A case study of the Yesanpo National Park. Plos one, 17(7), e0269841.

[5] Goger, B., Rotach, M. W., Gohm, A., Stiperski, I., & Fuhrer, O. (2016, July). Current challenges for numerical weather prediction in complex terrain: Topography representation and parameterizations. In 2016 international conference on high performance computing & simulation (HPCS) (pp. 890-894). IEEE.

[6] Wang, W., & Chen, F. (2025). Wind field modeling over hilly terrain: A review of methods, challenges, limitations, and future directions. Applied Sciences, 15(18), 10186.

[7] Cavalli, R., & Amishev, D. (2019). Steep terrain forest operations–challenges, technology development, current implementation, and future opportunities. International Journal of Forest Engineering, 30(3), 175-181.

[8] Cheng, J. (2025). Practice and application of three-dimensional modeling algorithm based on multi-source data fusion in geographic information systems. Journal of Computational Methods in Sciences and Engineering, 14727978251364468.

[9] Jebur, A. K. (2021). Uses and applications of geographic information systems. Saudi J. Civ. Eng, 5(2), 18-25.

[10] Kholoshyn, I., Nazarenko, T., Bondarenko, O., Hanchuk, O., & Varfolomyeyeva, I. (2021, March). The application of geographic information systems in schools around the world: a retrospective analysis. In Journal of physics: Conference series (Vol. 1840, No. 1, p. 012017). IOP Publishing.

[11] Sowmiya Narayanan, K. J., & Manimaran, A. (2024). Recent developments in geographic information systems across different application domains: a review. Knowledge and Information Systems, 66(3), 1523-1547.

[12] Janipella, R., Gupta, V., & Moharir, R. V. (2019). Application of geographic information system in energy utilization. In Current Developments in Biotechnology and Bioengineering (pp. 143-161). Elsevier.

[13] Hu, Q., Li, Z., Wang, L., Huang, Y., Wang, Y., & Li, L. (2019). Rainfall spatial estimations: A review from spatial interpolation to multi-source data merging. Water, 11(3), 579.

[14] Li, Z., Wang, H., Zhang, T., Zeng, Q., Xiang, J., Liu, Z., & Yang, R. (2023). Multi-Source Precipitation Data Merging for High-Resolution Daily Rainfall in Complex Terrain. Remote Sensing, 15(17), 4345.

[15] Jiang, H., Yang, Y., & Bai, Y. (2019). Using Multi-Source Data. Sustainable Directions in Tourism, 26.

[16] Huang, J., Wei, L., Chen, T., Luo, M., Yang, H., & Sang, Y. (2023). Evaluation of DEM Accuracy Improvement Methods Based on Multi-Source Data Fusion in Typical Gully Areas of Loess Plateau. Sensors, 23(8), 3878.